

# scientific data



**OPEN**  
DATA DESCRIPTOR

## Cytotoxic and Mechanical Properties of Resins 3D Printed with Low-Cost Hardware for C2C12 Biohybrid Actuators

Ashlee S. Liao , Kevin Dai , Alaeddin Burak Irez ,<sup>1,2,3</sup> Anika Sun , Michael J. Bennington , Saul Schaffer , Bhavya Chopra , Ji Min Seok , Rebekah Adams , Yongjie Jessica Zhang ,<sup>1,2</sup> & Victoria A. Webster-Wood ,<sup>1,2,4,5,6</sup>✉

For biohybrid actuators, the properties of synthetic materials interfacing with living cells are crucial due to cellular chemical and mechanical sensitivities. 3D-printable resins exhibit a wide range of properties, but mechanical properties are frequently reported before sterilization. Additionally, biocompatibility must be assessed for specific use cases, including in the context of the cell type and printing procedures. Therefore, this data descriptor details a new dataset of cytotoxicity and material properties of six commercially-available resins (three rigid and three elastomeric) printed on a Phrozen Sonic Mini 8K and sterilized using 70% ethanol exposure or autoclaving. Experiments were designed to model C2C12-biohybrid conditions. Cytotoxicity analyses were conducted by directly culturing C2C12 with sterilized samples. For material characterization, uniaxial tension and compression tests with post-hoc Hookean and Yeoh models and print fidelity assessments were conducted for nonsterile and sterile samples. The mechanical properties were assessed after submersion in phosphate-buffered saline to mimic conditions in biohybrid applications. Overall, this dataset provided comprehensive testing on cytotoxicity and material properties for 3D-printable resins in C2C12-biohybrid applications.

### Background & Summary

Biohybrid actuators integrate synthetic and organic materials to produce force and movement, which demonstrate potential for biomedical applications, such as regenerative medicine and pharmaceutical screening<sup>1,2</sup>. Since biohybrid actuators are reliant on the close relationship between synthetic and organic materials, selecting the appropriate nonliving materials to interface with the living materials is key to developing a functional system<sup>3</sup>. When selecting an appropriate synthetic material, key parameters to consider are material mechanical properties and biocompatibility<sup>3</sup>. With the advent of additive manufacturing, 3D-printable resins provide an accessible source of materials with a wide range of mechanical properties, enabling the rapid production of customized medical and biohybrid devices (select resins listed in Table 1). However, there is insufficient data publicly available on the cytotoxicity and the post-sterilization mechanical properties of most commercially available resins.

Although several commercially available resins are now available that have been advertised to be biocompatible<sup>(3,4)</sup>, and a subset can be found in Table 2), the International Organization for Standardization's (ISO) 10993 family of standards for biocompatibility requires that tests must be designed and implemented to assess biocompatibility in only specific material use cases instead of a general assessment to be interpreted for all potential uses<sup>5</sup>. Based on these standards, before any commercial resins are used for biohybrid applications,

<sup>1</sup>Department of Mechanical Engineering, Carnegie Mellon University, 5000 Forbes Ave, Pittsburgh, 15213, PA, USA.

<sup>2</sup>Department of Biomedical Engineering, Carnegie Mellon University, 5000 Forbes Ave, Pittsburgh, 15213, PA, USA.

<sup>3</sup>Department of Mechanical Engineering, Istanbul Technical University, Reşitpaşa, 34485 Sariyer, Istanbul, Turkey.

<sup>4</sup>Department of Materials Science and Engineering, Carnegie Mellon University, 5000 Forbes Ave, Pittsburgh, 15213, PA, USA. <sup>5</sup>Robotics Institute, Carnegie Mellon University, 5000 Forbes Ave, Pittsburgh, 15213, PA, USA. <sup>6</sup>McGowan Institute for Regenerative Medicine, University of Pittsburgh, 450 Technology Drive, Pittsburgh, 15219, PA, USA.

✉e-mail: [vwebster@andrew.cmu.edu](mailto:vwebster@andrew.cmu.edu)

Resin	Tensile Modulus (MPa)	Ultimate Tensile Strength (MPa)	Elongation at Break	Shore	Flexural Strength (MPa)	Flexural Modulus (MPa)
Formlabs Silicone 40A Formlabs <sup>35</sup>	Not Listed	5.0	230%	40A	Not Listed	Not Listed
3Dresyns Bioflex A10 MB 3Dresyns <sup>36</sup>	< 1	< 1	>> 300%	10A	< 1	Not Listed
Asiga DentaGUM	Not Listed 1.84 <sup>†</sup>	Not Listed 3.41 <sup>†</sup>	Not Listed	Not Listed	Not Listed	Not Listed
Asiga DentaGUIDE	Not Listed	Not Listed	Not Listed	Not Listed	Not Listed	Not Listed
Phrozen AquaGray 8K <sup>13</sup>	2433-2848	35–46	4.8–7.6%	80–86D	Not Listed	Not Listed
Liqcreate Bio-Med Clear Liqcreate <sup>34</sup>	2000	55	5–10%	85D	89* 80**	2200* 2500**

**Table 1.** Mechanical properties of commercially available, 3D printable resins as reported by their respective manufacturers. <sup>†</sup>For DentaGUM, Choi *et al.*<sup>33</sup> measured the elastic modulus and the tensile strength. For Liqcreate Bio-Med Clear Liqcreate<sup>34</sup>, the manufacturer's reported values are for samples \*after UV-cure (no steam sterilization) and \*\*after steam sterilization at 121°C.

Resin	Intended Use	Advertised Biocompatibility	Material Class
Formlabs Silicone 40A Formlabs <sup>37</sup>	Various, including medical	ISO 10993-5:2009 ISO 10993-10:2021 ISO 10993-23:2021	Elastomeric
3Dresyns Bioflex A10 MB 3Dresyns <sup>36</sup>	Biomedical applications	Biocompatible	Elastomeric
Asiga DentaGum Asiga <sup>38</sup>	3D Printed Gingiva Mask, Not for medical use	Not Listed	Elastomeric
Asiga DentaGuide Asiga <sup>38</sup>	3D-Printed Dental Surgical Guides, Short-term use (< 30 days)	CE Class I	Rigid
Phrozen AquaGray 8K <sup>13</sup>	General 3D Printing	Not Listed	Rigid
Liqcreate Bio-Med Clear Liqcreate <sup>34</sup>	Medical Devices	ISO 10993-5:2009 ISO 10993-10:2021 ISO 10993-23:2021	Rigid

**Table 2.** General overview of the use cases of six commercially-available, 3D-printable resins.

their biocompatibility should be reevaluated for their intended application<sup>3</sup>. Therefore, for the specific use in biohybrid actuators, in this analysis, a study was designed to assess the cytotoxicity of 3D-printable resins in direct contact with cultured muscle cells, specifically C2C12, when the resins were fabricated and cured using accessible manufacturing hardware.

Not only is there a need for cytotoxicity data when selecting a suitable resin for biohybrid actuator applications, but data on the mechanical properties is also crucial since there is a direct interface with living cells. Although the mechanical properties of printed resins are often freely available from manufacturers, synthetic materials must be sterilized before use with living cells. Sterilization methods for cell culture can impact mechanical properties and final print feature quality since they commonly utilize harsh conditions, such as high heat, high pressure, ultraviolet (UV) light exposure, or alcohols, such as ethanol or isopropanol, that can degrade resins<sup>6</sup>. Most resin manufacturers, even among the ones that produce biocompatible resins, do not report post-sterilization mechanical properties. Therefore, this study also includes resulting mechanical properties and printed feature quality for resins post-sterilization.

In addition to a diverse selection of commercially available resins, the rapid development of additive manufacturing technologies has led to various printers that range in printing feature resolution and cost. Currently, commercial 3D resin printers, which commonly use stereolithography (SLA) or digital light processing (DLP), can achieve resolutions on the order of tens of microns and a cost on the order of \$1000s USD<sup>7,8</sup>. For example, Asiga's DLP printer, MAX X27, can achieve a 27  $\mu\text{m}$  resolution<sup>9</sup> at a cost of \$9,990 as of April 2024<sup>10</sup>, and Formlabs' SLA printer for healthcare, Form 3B+, can achieve a 25  $\mu\text{m}$  XY resolution with an 85  $\mu\text{m}$  laser spot size<sup>11</sup> at a cost of \$4,429 as of April 2024<sup>12</sup>). With the increase in accessibility of resin printers entering the market for hobbyist crafters, the cost of high-resolution printers has drastically decreased to less than \$1,000 with the use of a liquid crystal display (LCD), also often referred to as masked stereolithography (MSLA)<sup>7,8</sup>. For example, Phrozen's Sonic Mini 8K LCD printer can achieve a 22  $\mu\text{m}$  resolution at a cost of \$485<sup>13</sup>. However, as these lower-cost printers enable open-source usage of third party resins, they commonly require more calibration and tuning per resin<sup>7</sup>. Additionally, 3Dresyns, a manufacturer of biocompatible resins, has noted that the light power of different printer models can impact the biocompatibility of the resulting printed product due to the risk of uncured monomers<sup>14</sup>. Therefore, the printer type and calibration conditions may affect the final cured resin product. In particular, if resins are under-cured due to the capabilities of the printer and curing station, residual monomers are likely to be present and are known to be cytotoxic. Thus, the biocompatibility and material properties must be reevaluated based on not only the resin and sterilization type but also the printer, curing, and wash approach used.

In this work, the cytotoxicity, mechanical properties, and print fidelity of six commercial resins (Table 3) were printed using a low-cost Phrozen Sonic Mini 8K and evaluated for biohybrid actuator applications when manufactured using this accessible, low-cost equipment. With the focus of evaluating accessible materials and equipment, which will not only lower the barrier to biohybrid research, but also improve reproducibility of experimental results across laboratories, only commercially available resins were considered. However, there are also a number of custom-made resins that could be considered if commercial options are not viable, but including custom resins were considered out of scope for this study to focus on accessibility and reproducibility.

Resin		Post-Print Treatment	Tensile Test	Compression Test
Rigid	Phrozen AquaGray 8K	IPA	ASTM D638 5 mm/min	ASTM D695 1.3 mm/min
	Liqcreate Bio-Med Clear	IPA		
	Asiga DentaGUIDE	IPA		
Elastomeric	Formlabs Silicone 40A	IPA IPA/BuOAc	ASTM D412 500 mm/min	ASTM D575 12 mm/min
	3Dresyns Bioflex A10 MB	IPA UNW2		
	Asiga DentaGUM	IPA		

**Table 3.** Resins used for the analysis with their associated post-print treatments and related mechanical testing standards used to guide their assessment. All resins had sample groups with identical isopropanol (IPA) treatment. Formlabs Silicone 40A and 3Dresyns Bioflex A10 MB were also assessed with a second sample group that was treated based on manufacturer's recommendations (80% IPA/20% *n*-butyl acetate (BuOAc) and UNW2, respectively).

Of the six resins in this study, three were considered rigid, and three were considered elastomeric to investigate a range of stiffnesses. The materials selected do not form an exhaustive list, but are aimed to provide the dataset with a range of properties to investigate materials that could be suitable either as rigid "skeletal"-like support structures or as flexible supports that would enable actuation and movement, which are both common applications in biohybrid actuators. Both mechanical testing and sample feature fidelity were evaluated for non-sterile and sterilized (autoclave or ethanol/UV) samples since material properties may change after sterilization. Cytotoxicity testing was only conducted with sterilized samples. Due to the inherent dependence of resin curing and, therefore, cytotoxicity on the printer and curing station parameters, these results should be interpreted in the context of using this low-cost, accessible equipment with the goal of broadening access to synthetic materials suitable for biohybrid robotics. For an initial analysis and application of this dataset for biohybrid actuators, refer to<sup>3</sup>, which focuses on the Asiga dental resins, and<sup>15</sup>, which covers the entire dataset.

## Methods

To identify suitable 3D-printable resins for biohybrid muscle-based devices, several commercial resins were characterized. These resins ranged in their mechanical properties (Table 1) and advertised biocompatibility (Table 2). However, the ISO 10993-1:2018 standard recommends that endpoint tests should be completed based on specific use cases<sup>5</sup>. Furthermore, all of the resins, with the exception of Liqcreate Bio-Med Clear, do not report mechanical properties after a sterilization treatment. Therefore, for the use case in biohybrid devices where there may be direct contact with cultured muscle cells and tissues, in particular, C2C12, the cytotoxicity, tensile, and compressive properties were measured and compared with and without common sterilization techniques used in biohybrid robotics.

**Sample Fabrication.** Six commercially available resins were selected for the analyses (Table 3). All resins were printed using a low-cost Phrozen Sonic Mini 8K resin printer (Phrozen Tech Co., LTD., Hsinchu, Taiwan). After printing, the samples were submerged in a container with 100% isopropanol (IPA) and placed in an ultrasonic bath for 5 minutes. This wash step was repeated once in a second container of 100% IPA. Each resin had its own dedicated first and second wash containers. After the two washes, the samples were dried and cured in a Phrozen Curing Station (405 nm UV lights, 60–80 mW/cm<sup>2</sup> (personal communication with manufacturer); Phrozen Tech Co., LTD., Hsinchu, Taiwan) with a fan period of 30 minutes followed by a cure period of 15 minutes. Then, the samples were flipped and cured for another 15 minutes. It is important to note that this printer, while broadly accessible due to its low cost, has a lower UV light intensity than other, less accessible, commercially available systems. For example, the Phrozen Sonic Mini 8K is reported to have a light intensity of less than 3 mW/cm<sup>2</sup>, whereas the Formlabs Form 4 has a 16 mW/cm<sup>2</sup> light intensity<sup>16</sup>. Therefore, the tests reported here should only be interpreted in the context of using such equipment as lower power systems have a higher risk of resulting in under-cured resins, which are known to present cytotoxicity risks. However, characterizing the cytotoxicity, mechanical properties, and print fidelity using a low-cost resin printer will expand the accessibility of these resins.

For two of the resins, Formlabs Silicone 40A and 3Dresyns Bioflex A10 MB, the respective manufacturers recommended alternative post-processing. Therefore, in addition to the IPA-processed samples, additional samples were fabricated for these resins and post-processed using their manufacturers' protocols. The additional Formlabs Silicone 40A samples were washed using the ultrasonic bath in an 80% IPA and 20% *n*-butyl acetate (BuOAc) solution. To wash the samples, the samples were placed in a container filled with IPA/BuOAc. This container was placed in an ultrasonic water bath for 10 minutes. This was repeated once in a second IPA/BuOAc container for a total of two wash cycles. After the washes, the samples were dried in the Phrozen Curing Station (405 nm UV light, 60–80 mW/cm<sup>2</sup> (personal communication with manufacturer); Phrozen Tech Co., LTD., Hsinchu, Taiwan) with a 15-minute fan period. Afterward, they were transferred to a Petri plate filled with water and cured in the Phrozen Curing Station (Phrozen Tech Co., LTD., Hsinchu, Taiwan) for 45 minutes. Lastly, they were removed from the water and stored in dry Petri plates before sterilization or testing.

For the second set of 3Dresyns Bioflex A10 MB samples, samples were washed twice in containers filled with Cleaning Fluid UNW2 Bio (UNW2) (P20759; 3Dresyns, Barcelona, Catalonia, Spain) for 5 minutes each in an ultrasonic bath. After the washes, the samples were cured in the Phrozen Curing Station (Phrozen Tech Co., LTD., Hsinchu, Taiwan) for 6 minutes while submerged in UNW2. Then, the samples were briefly dipped in IPA and allowed to dry. The duration in IPA was not timed and ranged from a few seconds to a couple of minutes as

individual samples were removed from the IPA in a random order to dry on a paper towel. Afterward, they were submerged in UNW2 for 1 hour at 65°C. Finally, they were submerged in deionized water for 1 hour at 65°C. After the final post-printing process, the samples were removed from the water and stored in dry Petri plates until they were sterilized or used for testing.

In addition to the resin samples, polydimethylsiloxane (SYLGARD 184; Dow Corning, Midland, MI, USA) with a 10:1 base-to-curing-agent (w/w) ratio was used as a reference standard (common material used in biohybrid actuators) in the biocompatibility assays. PDMS was cast in a Petri plate and cured for 6 hours at 65°C (master sample). After the PDMS was cured, cylindrical samples were cut from the master sample using a 2-mm biopsy punch.

For consistency, all of the resins post-processed with the same IPA washes and curing procedure were simultaneously assessed for cytotoxicity. Since the Formlabs Silicone 40A samples were also assessed with an alternative, manufacturer's post-processing procedure (IPA/BuOAc), the cytotoxicity assessment of these samples was done in a separate culture period than the assessment for the other IPA-processed resins. Therefore, separate PDMS control samples were used for this group. The PDMS samples were cut from the same master sample using a 2-mm biopsy punch.

**Sample Sterilization.** To sterilize the resins, two common methods of sterilization used in biohybrid robotics were explored: (1) autoclaving and (2) submersion in 70% ethanol with UV exposure. For autoclaving select samples, a gravity cycle at 121°C for 45 minutes with 15 minutes of dry time was used (ADV-PRO; Consolidated Sterilizer Systems, Billerica, MA, USA).

For the ethanol/UV sterilization method, samples were submerged in 70% ethanol for 1 hour at room temperature. Afterward, they were swirled three times in 1X phosphate-buffered saline (PBS, 10-010-049; Gibco ThermoFisher, Waltham, MA, USA) and, then, left to dry overnight in the biosafety cabinet (1300 Series A2, Model 1377; ThermoFisher, Waltham, MA, USA) with 1 hour of ultraviolet (UV) light exposure from the biosafety cabinet's regular sterilization cycle.

**Cytotoxicity Analysis.** Following the manufacturing process described above, a biocompatibility analysis was conducted to identify 3D-printable resins that can be used in direct contact with cultured cells over several days or weeks when produced with the low-cost equipment tested in this work. The appropriate biocompatibility analysis for this specific use was determined based on guidance from the International Organization for Standardization (ISO) "Biological Evaluation of Medical Devices" standards 10993-1:2018<sup>5</sup>, 10993-5:2009<sup>17</sup>, and 10993-12:2021<sup>18</sup>. Based on 10993-1:2018<sup>5</sup>, the use case was considered for prolonged periods of exposure (24 hours to 30 days), cytotoxicity tests with cell culture would be appropriate evaluation in line with ISO 10993-5:2009<sup>17</sup>, and samples should be prepared based on ISO 10993-12:2021<sup>18</sup>.

Based on 10993-5:2009<sup>17</sup>, a direct contact test was determined to be the appropriate analysis for prolonged exposure to cultured cells. The established mouse myoblast cell line, C2C12 (CRL-1772; ATCC, Manassas, Virginia, USA), was selected as a commonly established cell line for biohybrid muscle-based devices. For contact with the cells, cylindrical samples (2.2 mm diameter, 1.5 mm height) were fabricated with a flat face that occupied approximately 10% of the surface area of a single well of a 96-well plate. The positive control used was 70% ethanol since it will cause a cellular response - in this case, cell death. The reference standard used was PDMS samples (~2.34 mm height) created in 10:1 (w/w) ratio of base:curing agent and a 2-mm biopsy punch (refer to Section [Sample Fabrication](#)).

**Cell Culture.** Cryopreserved C2C12 cells were thawed and plated in 96-well plates (655087; Greiner Bio-One, Kremsmünster, Austria) at a density of 2,100 cells/well. The plating time corresponded with the beginning of the 9th passage for the cells. C2C12 growth media composed of high-glucose Dulbecco's Minimum Essential Medium (DMEM, 11965126; Gibco ThermoFisher, Waltham, MA, USA) supplemented with 10% fetal bovine serum (A5256801; Gibco ThermoFisher, Waltham, MA, USA), 1% penicillin/streptomycin (10,000 U/mL, 15140122; Gibco ThermoFisher, Waltham, MA, USA), and 1% L-glutamine (200 mM, 25030081; Gibco ThermoFisher, Waltham, MA, USA). The cells were cultured for 2 days before a complete media change and the introduction of resin samples. To expose the cells to the resin, the samples were gently placed on top of the monolayer of cells using forceps. Cytotoxicity measurements were taken 72 hours after the introduction of resin samples. There were 6 replicate wells for each resin type, the reference standard (PDMS), the positive (70 % ethanol) controls, and the blank (cell only, no resin exposure) controls. PDMS was selected as the reference standard as the material is generally considered biocompatible<sup>19</sup>. Although there are some studies that demonstrate the possibility of leaching oligomers from uncured PDMS that impact certain cellular functions<sup>20,21</sup>, PDMS has been used as a common material for biohybrid actuators composed of C2C12, resulting in contractile mechanisms<sup>22–24</sup>. Therefore, in the application of C2C12 biohybrid actuators, PDMS was considered an appropriate reference standard for this cytotoxicity study, but further investigation into impacts on contractility should be considered.

**Cytotoxicity (Plate Reader and Imaging).** Cytotoxic effects were measured using ThermoFisher LIVE/DEAD Viability/Cytotoxicity Kit (L3224; Invitrogen ThermoFisher, Waltham, MA, USA), which uses fluorescence dyes calcein-AM and ethidium homodimer-1 for identifying live and dead cells, respectively. For the wells with samples and the reference standard (PDMS), before washing the cells and applying the dyes, all of the resin samples were carefully removed to minimize the risk of cells detaching from the culture surface due to the movement of the samples during the wash steps. For the positive controls, the media was first aspirated and replaced with cold 70% ethanol and incubated at room temperature for at least 15 minutes prior to the wash steps.

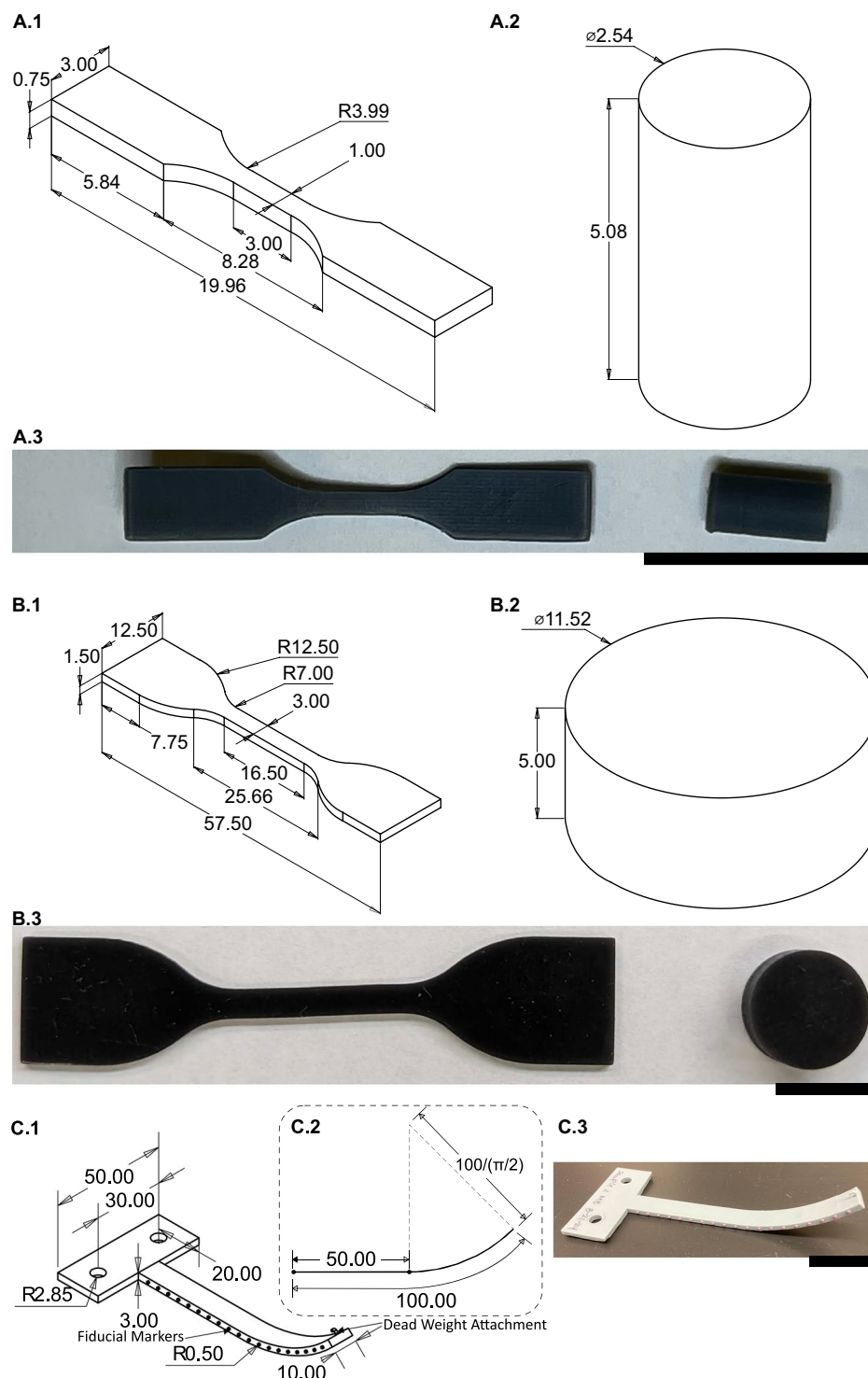


**Fig. 1** Specimen samples for the (A) rigid resin samples as per ASTM D638 and ASTM D695 recommendations and for the (B) elastomeric resin samples as per ASTM D412 and ASTM D575 recommendations. (1) Tensile sample specifications. (2) Compression sample specifications. The drawings are not to scale with respect to each panel. (3) Actual samples of (A.3) Phrozen AquaGray 8K and (B.3) Formlabs Silicone 40A with IPA-post-treatment. Scale bars represent 10 mm. Refer to supplementary materials for detailed files. (C) Precurved cantilevered beam used in follow-up mechanical testing. (1) Isometric CAD drawing of the beam. Dead weights were hung by Kevlar threads to the dead weight attachment, and the fiducial markers were painted with acrylic paint to enhance contrast. (2) Centerline geometry of the beam centerline. This geometry was generated in MATLAB and exported as a 3D curve to SolidWorks. (3) Actual sample of a Phrozen AquaGray 8K beam. Scale bar is 40 mm.

After sample removal, the wells were washed three times with 1X PBS. After the last rinse, 100  $\mu\text{L}$  of 1X PBS was added to each well. For the wells that contained the samples and the reference standard wells, 100  $\mu\text{L}$  of the dye solution containing 1  $\mu\text{M}$  calcein-AM and 2  $\mu\text{M}$  of ethidium homodimer-1 was added to each well. For the positive and blank controls, 100  $\mu\text{L}$  of only 1  $\mu\text{M}$  calcein-AM was added to half of the wells, and 100  $\mu\text{L}$  of only 2  $\mu\text{M}$  ethidium homodimer-1 was added to the remaining half, as recommended by the manufacturer's protocol<sup>25</sup>.

After 30 minutes of incubation, the fluorescence was measured using a plate reader (Synergy H1; Agilent BioTek, Santa Clara, CA, USA) using the fluorescence endpoint test of the entire well, read from the bottom of the well plate, for each sample. A monochromator with a xenon flash light source with high lamp energy, extended gain, and extended dynamic range was used with two filter sets: (1) default "Calcein" setting (485 nm excitation, 526 nm emission) and (2) default "Texas Red" setting (584 nm excitation, 625 nm emission). For the measurements, a normal read speed was used with a 100 ms delay, 10 data point measurements per well, and a 7 mm read height. During the measurements, the plate lids of the 96-well plates were still used. For the analysis, the ratio of calcein AM fluorescence and ethidium homodimer-1 (Texas Red) fluorescence (CalAM:EthD-1) was used.

Quantitative assessment of the cytotoxicity can be completed on the fluorescence readings from the plate reader. In particular, when using calcein AM and ethidium homodimer-1 as the method for determining cell viability, analyzing the ratio of calcein AM to ethidium homodimer is more appropriate for analysis than using individual fluorescence intensities to quantify living and dead cells<sup>26</sup>. This quantitative data can be used for making informed choices in selecting resins to be used in direct contact with C2C12 cells. In addition to the quantitative measures reported in this dataset, to qualitatively validate the quantitative measurements from the plate reader, once the plate was read, the wells were imaged using a 5 MP sCMOS mono camera on an inverted Echo Revolution microscope under epifluorescence with the FITC and TXRED LED light cubes at 10X magnification (Revolution; Echo Bico, San Diego, CA, USA).

**Materials Characterization.** To assess the effects of the sterilization method (refer to Section [Sample Sterilization](#)) on the mechanical properties of each resin, tensile and compression tests (Table 3) were conducted on nonsterile, ethanol/UV-sterilized, and autoclaved samples (Fig. 1). Prior to the tests, the samples were conditioned in 1X PBS at 37°C for 16 hours. The PBS conditioning was crucial to mimic biohybrid application conditions where materials may be submerged in cell culture media when in contact with cells for extended periods of time. The tests were performed using an MTS Criterion Model 42 (C42) Universal Test Stand. Furthermore, during testing, the samples were maintained in 1X PBS at 37°C using an MTS Bionix EnviroBath. Just before inserting each sample into the grips for testing, the rest geometry of each sample was measured using Neiko digital calipers. For compression samples, the gauge length was measured as the full height of the puck. For tensile samples, the gauge length was measured as the grip separation after the sample was installed into the machine. Testing protocols for the tensile and compression tests were based on ASTM standards D695-23 (rigid compression), D575-91 (elastomeric compression), D638-14 (rigid tensile), and D412-06a (elastomeric tensile). The protocols in these standards are briefly summarized here:

**Rigid Compression Test.** Compression tests were conducted on rigid samples (Fig. 1A.2), with six samples tested from each group. For the testing, sandpaper was applied to both the lower and upper compression plates to prevent the samples from slipping. Subsequently, the samples were positioned at the center of the bottom plate, and their alignment with the upper plate was verified. Next, mild contact was made between the upper plate and the specimen by slowly adjusting the crosshead until a negligibly small load (0.05–0.1 N) was registered. During this stage, careful consideration was given to ensuring that no load was transferred to the specimen before conducting the tests. Subsequently, the test was commenced, and it was promptly halted when the force hit 48 N. Any force greater than 50 N has the potential to cause damage to the 50-N-load cell in the test machine. Consequently, the test was concluded at 48 N, and the test data was recorded.

**Elastomeric Compression Test.** Elastomeric compression tests were performed on the specimens shown in Fig. 1B.2. The test was conducted utilizing the identical experimental configuration as the rigid compression tests. The test was conducted in three stages once the upper plate made slight contact, as indicated by the registration of a negligibly small load (0.05–0.1 N), with the test material. During the initial phase, a force of 1 N was applied to the sample at a testing rate of 1.3 mm/min. Once the force of 1 N was reached, in the subsequent phase, the upper plate of the test device remained stationary for a duration of 30 seconds. During the third step, a force was exerted at a constant test speed (Table 3) until it achieved a magnitude of 40 N. The test was subsequently halted. Only the data from the third stage was captured during this test, complying with the ASTM D575 test standard.

**Rigid Tensile Test.** Rigid tensile tests were performed on the samples shown in Fig. 1A.1. Sandpaper was applied to the interior surfaces of the test grips to keep samples from slipping during testing, and samples were placed between the grips. This procedure ensured that the samples were properly aligned between the grips, which is critical for the tests' uni-axial tensile nature. After inserting the specimen and ensuring alignment with the testing axis, the distance between the grips (gauge length) was measured using calipers. The strain could not be measured using strain gauges or any other contact extensometer since the sample size was so small. Tests were then performed using displacement control at a crosshead speed of 5 mm/min (ASTM D638), with a 48 N force limit applied to avoid damaging the test machine's 50-N-load cell.

Resin		Compressive Modulus	Young's (Tensile) Modulus	Ultimate Tensile Strength	Elongation at Break	Stress at 50% Strain	Stress at 100% Strain
Rigid	Asiga DentaGUIDE	✓	✓	✓	✓		
	Liqcreate Bio-Med Clear	✓	✓	✓	✓		
	Phrozen AquaGray 8K	✓	✓	✓	✓		
Elast.	3Dresyns Bioflex A10 MB			✓	✓	✓	
	Formlabs Silicone 40A					✓	✓
	Asiga DentaGUM			✓	✓	✓	✓

**Table 4.** Mechanical properties measured for each rigid and elastomeric (Elast.) resin. For rigid resins, stress at 50% and 100% strain was not considered as they break before achieving 50% strain. For 3Dresyns Bioflex A10 MB, the samples broke before achieving 100% strain. The ultimate tensile strength and elongation at break was not calculated for Formlabs Silicone 40A since a majority of those samples (32 of 36 samples) did not break due to machine limits. The compressive and tensile moduli were not calculated for elastomeric resins due to their hyperelasticity.

*Elastomeric Tensile Test.* Elastomeric tensile tests were performed on the samples shown in Fig. 1B.1. The most important aspects of these tests were correct sample alignment and maintaining the sample completely parallel to the vertical axis of the testbed (direction of force application) without loading it. After aligning the specimen and keeping it parallel to the vertical axis, the gauge length was measured using a caliper, and the test proceeded. The sample was stretched at a constant crosshead speed of 500 mm/min (ASTM D412). The test ended after either a complete failure or nearing the physical limits of the EnviroBath cabinet.

*Data Analysis and Modeling.* During all testing protocols, material displacement and reaction force were recorded by the MTS at 10 Hz. From these data, engineering stress ( $\sigma_{eng}$ : force / rest cross sectional area) and strain ( $\epsilon$ ) were calculated. For the dogbone samples, strain was calculated relative to the gauge length of the sample. For consistency between the different protocols with different durations (and thus different numbers of data points), the stress and strain data were resampled at 50 equally spaced strain values, and analysis was performed on these resampled data.

In addition to the raw stress and strain data for these materials, a catalog of characteristic material properties and model parameters was created for these materials and fabrication conditions. These values include stiffness parameters and failure characteristics, which can be used both in mechanical models of structures fabricated with these materials and to inform an appropriate material choice for a given biohybrid design. Both the raw data and the property catalog are provided to allow researchers to fit their own material models to the data or to utilize a robustly calibrated and validated material model in their analyses. Additionally, the analysis performed below can be used as a template for other such analyses, either for new materials or for the reanalysis of the data presented here.

For the rigid samples, the Young's modulus was calculated based on the ASTM D638 (Table 3). For consistency across samples with differently-shaped stress-strain curves, the ASTM standards for materials with no linear region were utilized. Briefly, from the stress-strain data, the slope between adjacent points was calculated and then smoothed with a 10-point moving average filter. The location of the maximum instantaneous slope was chosen as the linear region, and a linear function was fit to the surrounding 3 points. To account for the toe region in the data, the x-axis intercept of this line was then used as the zero point for the stain, and the strain data were adjusted accordingly. Finally, the slope of this line was recorded as the Young's (or Compressive) Modulus of that sample. In addition to the modulus, for tensile tests, the Ultimate Tensile Strength (UTS) and Strain at Break were measured for each sample as the maximal stress and strain values, respectively. This procedure was followed for all rigid samples (Table 4).

For the elastomeric material samples, a simple linear elastic model was insufficient to capture their elastic response. Instead, an incompressible Yeoh hyperelastic model was fit to the data<sup>27</sup>. The strain energy density function ( $\Psi$ ) of the Yeoh model used here takes the form:

$$\Psi(I_1) = C_1(I_1 - 3) + C_2(I_1 - 3)^2 + C_3(I_1 - 3)^3 \quad (1)$$

where  $I_1$  is the first invariant of the Cauchy deformation tensor ( $I_1 = \lambda_1^2 + \lambda_2^2 + \lambda_3^2$ , where  $\lambda_i$  is the  $i^{th}$  principle stretch), and  $C_j$  are material parameters that were fit from the data. For the uniaxial experiments performed here,  $\lambda_1 = \lambda = 1 + \epsilon$  and, from incompressibility,  $\lambda_2 = \lambda_3 = \lambda^{-0.5}$ . The engineering stress for the material can then be calculated (taking into account the hydrostatic pressure associated with the incompressibility constraint) as

$$\sigma_{eng} = 2(\lambda - \lambda^{-2})(C_1 + 2C_2(I_1 - 3) + 3C_3(I_1 - 3)^2) \quad (2)$$

For uniaxial tests,  $I_1 = \lambda^2 + 2/\lambda$ . The equivalent Young's Modulus can be calculated from the model parameters as  $E = 6C_1$ <sup>27</sup>. As with the rigid material, the toe region of the data was ignored. However, a similar standard procedure for doing so was not present for elastomeric materials. Instead, all stress below 5% of the max stress was considered potential toe region. Then, to adjust the strain levels, it was assumed that the beginning of the data was still in an approximately linear region. The first five data points were fit to a line ( $\sigma = a\lambda + b$ ), and a

Feature	Ground Truth Score
Column Containing the Largest Feature	1
Column Containing the Smallest Feature	7
Row Containing the Largest Feature	A
Row Containing the Smallest Feature	G
Print Fidelity (Entire Sample)	5
Print Fidelity (Quadrant 1)	5
Print Fidelity (Quadrant 2)	5
Print Fidelity (Quadrant 3)	5
Print Fidelity (Quadrant 4)	5

**Table 5.** Table of each scored feature and the associated ground truth score.

Resin	Phrozen AquaGray 8K	Liqcreate Bio-Med Clear
Manufacturer-Reported Stiffness [MPa]	2433–2848 <sup>13</sup>	2000 <sup>34</sup>
Measured Tensile Modulus [MPa]	382 ± 37	708 ± 50
	Sample 1	Sample 2
Non-Soaked Beam Young's Modulus [MPa]	2440 ± 98	2400 ± 96
Pre-Soaked Beam Young's Modulus [MPa]	440 ± 18	400 ± 16
	1970 ± 79	1650 ± 66
	1130 ± 45	1210 ± 48

**Table 6.** Effects of PBS Pre-Soak on Resin Stiffness. “Measured Tensile Modulus” values were measured using the tensile tests described above. Two beams were tested for each resin and soaking condition, and the Young’s modulus for each is reported. Errors were determined from a convergence analysis of the beam model.

displacement offset was calculated as  $\delta L = L_0(b/a + 1)$ , where  $L_0$  is the gauge length of the sample. This offset  $\delta L$  was then subtracted from the measured displacement, and the adjusted stretch was recalculated. This adjusted stretch was used for model fitting.

To ensure that the same model properly captured compression and tensile tests, the model parameters were calibrated using compression and tensile data simultaneously. However, tensile and compression data are not available for the same specimen. To overcome this limitation, a bootstrapping approach was utilized. For each step of the bootstrap, one compression and one tensile dataset were sampled to construct a dual-side stress-strain curve. Then, the three material parameters were fit by minimizing the squared error between the model and experimental data using MATLAB’s *fminsearch* optimization function. Penalty terms were added to ensure  $C_1$  and  $C_3$  were greater than 0 for stability, but  $C_2$  was allowed to be positive or negative<sup>27</sup>. These model parameters were then logged, and this process was repeated 50 times. The mean model response was then calculated as the model response given the mean model parameters. This is possible because the strain energy model is linear in its parameters. To determine the goodness of fit for the mean models, the coefficient of determination ( $R^2$ ) was calculated using all experimental data.

Scalar metrics were also calculated for the elastomer samples. UTS and Strain at Break could only be calculated for a subset of samples because not all samples failed during testing (Table 4). Additionally, to align with metrics reported by select manufacturers, we calculate the stress at 50% and 100% (when possible) strain. This was found for each sample by linearly interpolating the experimental data and sampling at stretches of 1.5 and 2. For samples that did not reach 50% or 100% strain before the end of the test, no stress was calculated for that sample.

*Effect of PBS Pre-Soaking.* For all mechanical experiments described above, the rigid resin samples were incubated in 1X PBS at 37°C for 16 hours. However, it was observed that the Young’s moduli calculated from our tests were consistently lower than those reported by the manufacturers (Table 6). To test if this was caused by the PBS incubation, we performed follow-up mechanical tests using curved cantilevered beams (Fig. 1(c)). Beams were printed in Phrozen AquaGray 8K and Liqcreate Bio-Med Clear using the same parameters and post-processing as the prior samples. Beams were not tested in Asiga DentaGUIDE because a stiffness was not provided by the manufacturer for comparison. For each resin, two samples were tested immediately after post-processing and two samples were subjected to the PBS incubation before testing. In these tests, the beams were fixed on one end and vertically loaded on the other with 0g (no weight), 100g, and 200g dead weights sequentially. Images were taken, and the locations of fiducial markers were digitized using WebPlotDigitizer<sup>28</sup>. Then, from these data, the Young’s modulus was approximated by fitting a geometrically exact Euler-Bernoulli beam model<sup>29,30</sup> (See<sup>29</sup> for model derivation). For these experiments, it was assumed that the axial force ( $N$ ) and bending moment ( $M$ ) both followed linear constitutive laws as follows:

$$N(s) = EA\epsilon(s) \quad (3)$$

and

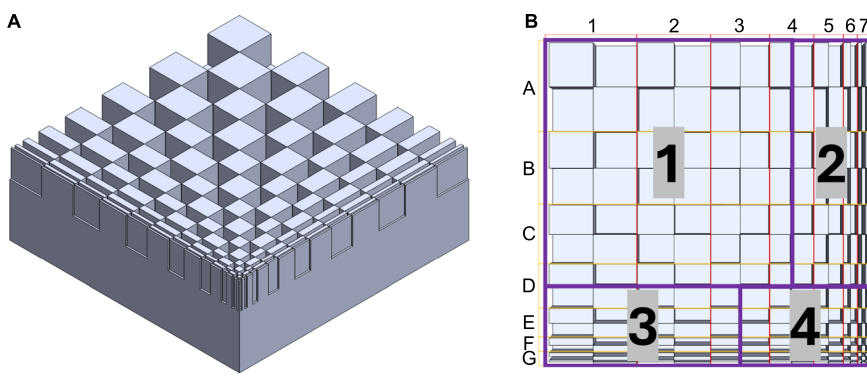


**Fig. 2** The printed samples had an alternating pattern of raised rectangles with decreasing length and width. The largest feature (Row A, Column 1) had a length and width of 0.6mm and the smallest feature (Row G, Column 7) had a length and width of 0.025 mm. (A) Isometric view of the print fidelity sample CAD model (B) Row, column, and quadrant labels of the top face of the print fidelity sample. These labels tag regions are used for the manual assessment of feature quality. All scale bars represent 1 mm. The detailed CAD models are included as part of the associated repository.

$$M(s) = EI \frac{\partial}{\partial s} (\theta(s) - \theta_0(s)) \quad (4)$$

where  $E$  is the unknown Young's modulus,  $A$  is the cross-sectional area and  $I$  is the second moment of area (both calculated from the prescribed geometry),  $\epsilon(s)$  is the strain, and  $\theta(s)$  is the tangent angle to the horizontal. Here, the beam is parameterized by the arclength  $s$ .  $\theta_0(s)$  is the rest angle of the beam to account for the resting curvature. The model equations were solved using a Finite Difference approach. The Young's modulus was found by minimizing the squared error between the model and experimental data for the 100g and 200g tests simultaneously. The error in the Young's modulus was approximated from a previously conducted convergence test on the beam model.

**Print Fidelity.** To assess the print fidelity for each resin using our low-cost 3D printer, samples with feature sizes ranging from 25  $\mu\text{m}$  to 600  $\mu\text{m}$  were printed (Fig. 2). Only the XY resolution was assessed for this study, but future studies should explore Z-resolution if more complex geometries are needed. The samples were fabricated and sterilized as described in Sections [Sample Fabrication](#) and [Sample Sterilization](#). For the print fidelity assessment, the individual nonsterile, ethanol/UV-sterilized, and autoclaved samples were imaged using a 10MP CMOS camera on an AmScope SM-1T trinocular stereo microscope with a ring light and without a Barlow lens (SM-1TSZZ-144S-10M, AmScope). The samples were then analyzed by three co-authors for feature size and overall fidelity according to a set scoring rubric using Likert-type scales. The scorers were asked to select the location of the largest and smallest features by sectioned column and row. The scorers were also asked to rank overall print fidelity and print fidelity in quadrants on a 0-5 scale (0: no features visible; 5: all the features are identical to the target model from the CAD file). The quadrants were selected to distribute the number of features evenly, with quadrant 1 containing the largest features and quadrant 4 containing the smallest (Fig. 2). CAD files and additional experimental images can be found in the data repository associated with this work. The ground truth score for each feature is collected in Table 5. Both the images of all the samples and resulting scores can be reanalyzed to assess the print qualities under all of the experimental conditions.

### Data Records

All data, CAD files, and code associated with this work can be found in the associated online Zenodo repository<sup>31</sup>, <https://doi.org/10.5281/zenodo.15801032>. The raw cytotoxicity data was directly exported from the plate reader software as a spreadsheet. The raw mechanical testing data was also exported as a spreadsheet. All of the trials from the mechanical testing were combined into one master spreadsheet. In addition, the images from the stereo microscope and the associated responses as a spreadsheet for the print fidelity manual assessment are also included in the repository. The “README.md” document details all of the content for this dataset.

### Technical Validation

**Controls for Cytotoxicity Analysis.** For the cytotoxicity assessment, several controls and replicates were used for the technical validation of the dataset (refer to Section [Cell Culture](#)). The microscopy images were used only to qualitatively validate the cell staining process. To validate the cell staining process, the blank control in which there was no exposure to any additional substances beyond the cell culture media was expected to exhibit a strong calcein AM fluorescence with minimal ethidium homodimer-1 fluorescence. In addition, the positive control with exposure to 70% ethanol, which was expected to cause cell death, should only exhibit fluorescence due to ethidium homodimer-1. The microscopy images qualitatively indicated that these controls exhibited expected fluorescence (Figs. 3, 4). Surprisingly, the procedure of washing the cells with PBS and loading them

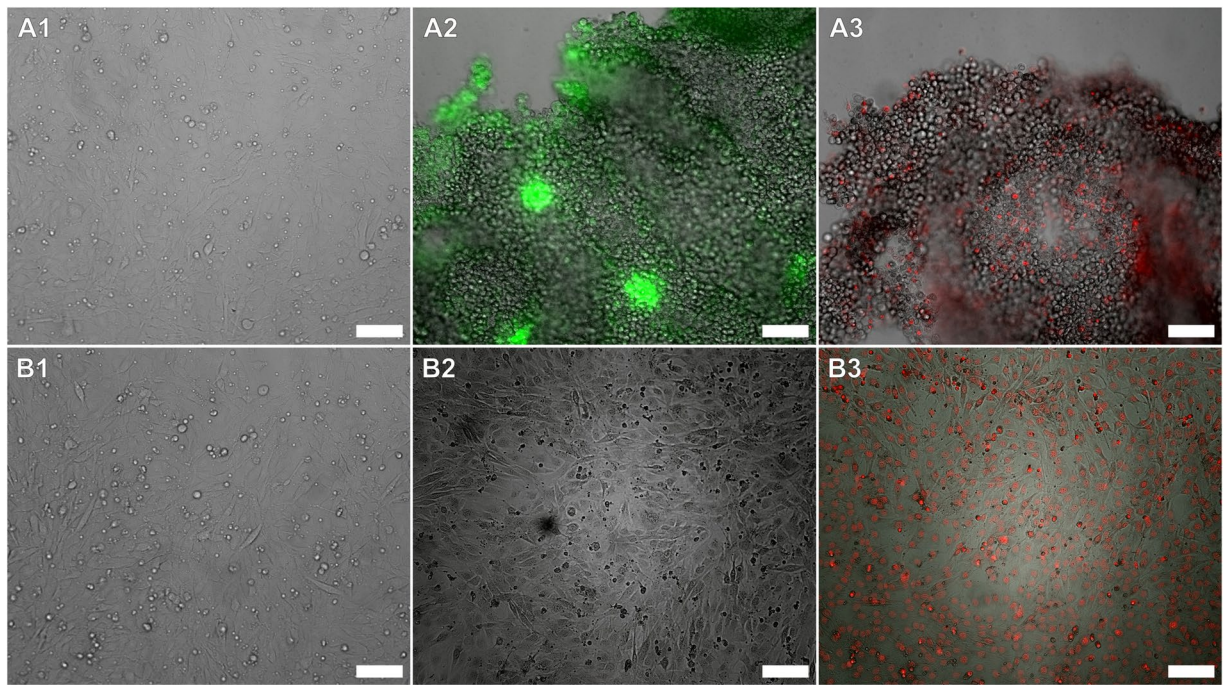


**Fig. 3** Brightfield and fluorescence microscopy images of cells that were not exposed to any resin samples. These controls were used for the biocompatibility assessment of all resins except for the Formlabs Silicone 40A post-treated with IPA/BuOAc. (A) represent the blank (live cell) controls. (B) represent the positive (dead cell) controls, with (B1) illustrating the cells prior to incubation with 70% ethanol. (1) are brightfield-only images of the cells prior to loading of any dye. (2) are brightfield images overlaid with fluorescence images of cells loaded only with calcein AM (green). (3) are brightfield images overlaid with fluorescence images of cells loaded only with ethidium homodimer-1 (red). All scale bars are 100  $\mu\text{m}$ .

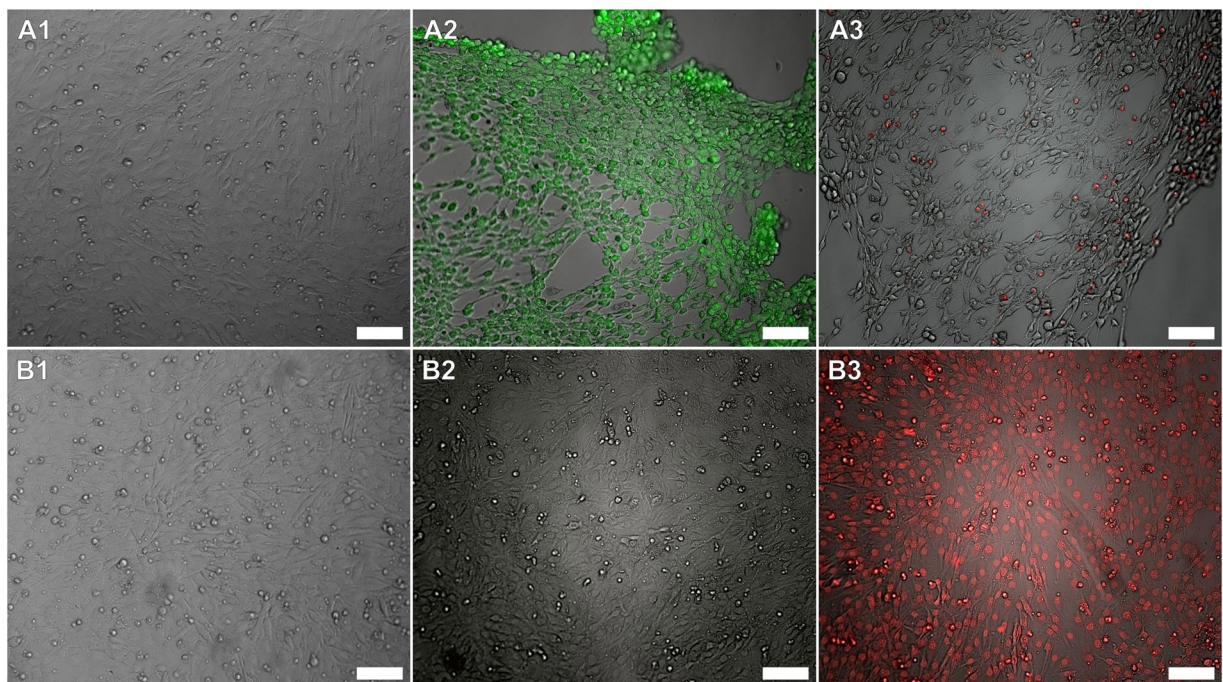


**Fig. 4** Brightfield and fluorescence microscopy images of cells that were not exposed to any resin samples. These controls were used for the biocompatibility assessment of the Formlabs Silicone 40A post-treated with IPA/BuOAc. (A) represent the blank (live cell) controls. (B) represent the positive (dead cell) controls, with (B1) illustrating the cells prior to incubation with 70% ethanol. (1) are brightfield-only images of the cells prior to loading of any dye. (2) are brightfield images overlaid with fluorescence images of cells loaded only with calcein AM (green). (3) are brightfield images overlaid with fluorescence images of cells loaded only with ethidium homodimer-1 (red). All scale bars are 100  $\mu\text{m}$ .

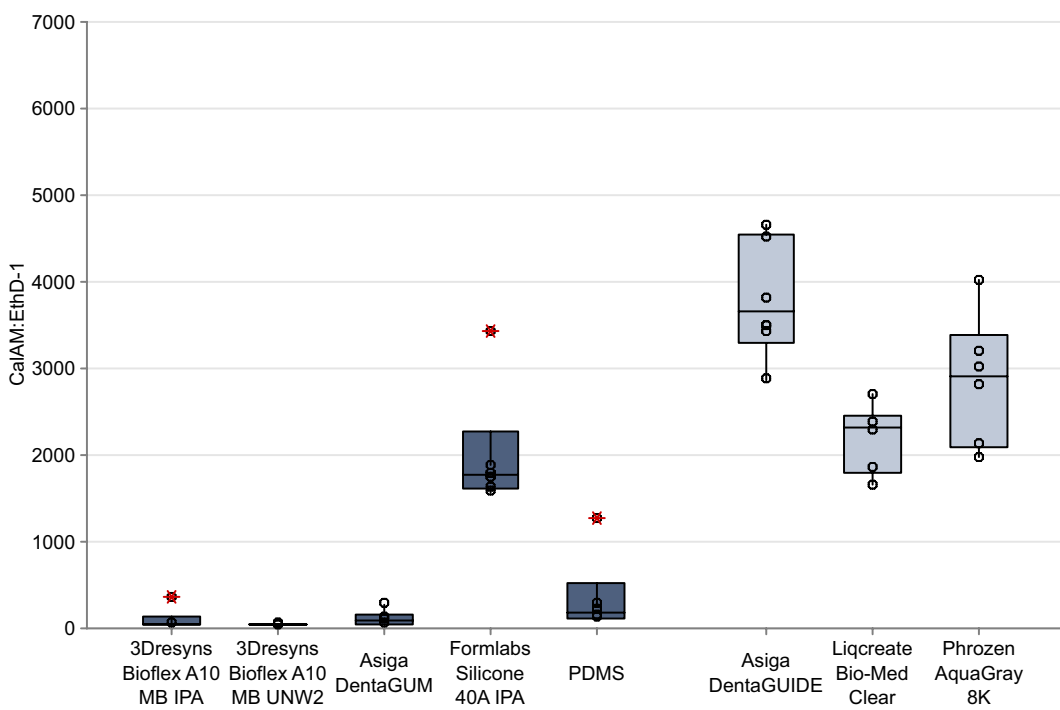


**Fig. 5** The CalAM:EthD-1 responses represented as boxplots of the ethanol/UV-sterilized rigid (dark blue-gray) and elastomeric (light blue-gray) resin samples, excluding the Formlabs Silicone 40A post-treated with IPA/BuOAc. Open circles (○) represent individual data points. The red asterisks (\*) denote outliers. The upper and lower boundaries of the box represent the first and third quartiles. Whiskers extend from the interquartile boxes to the minimum and maximum values, excluding outliers.

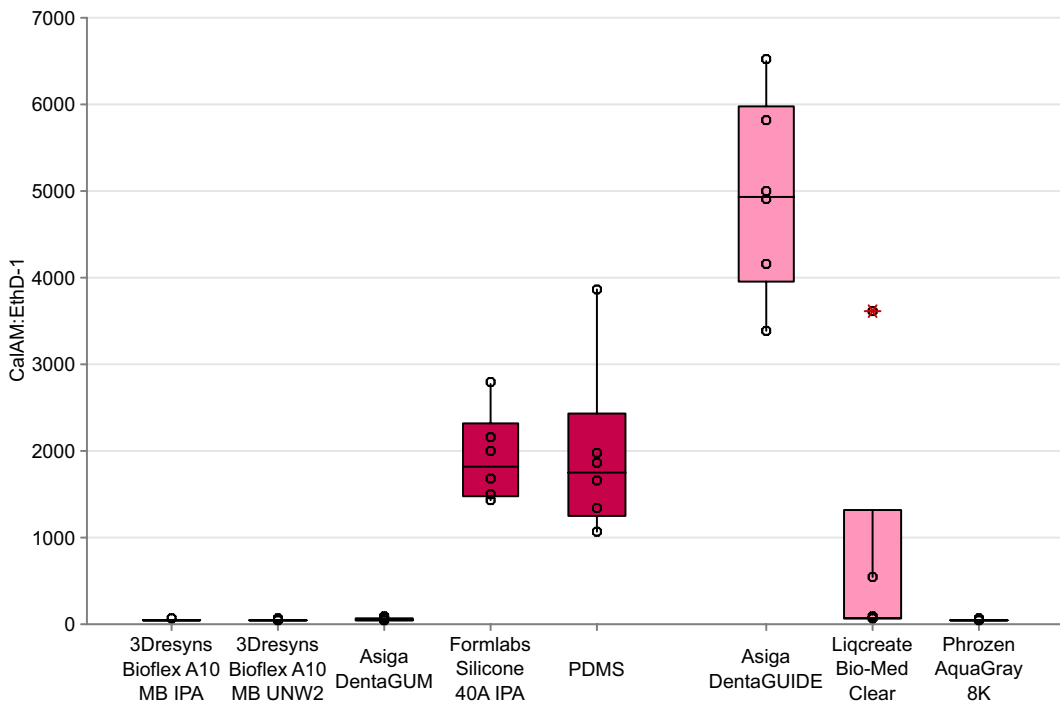


**Fig. 6** The CalAM:EthD-1 responses represented as boxplots of the autoclaved rigid (dark pink) and elastomeric (light pink) resin samples, excluding the Formlabs Silicone 40A post-treated with IPA/BuOAc. Open circles (○) represent individual data points. The red asterisks (\*) denote outliers. The upper and lower boundaries of the box represent the first and third quartiles. Whiskers extend from the interquartile boxes to the minimum and maximum values, excluding outliers.

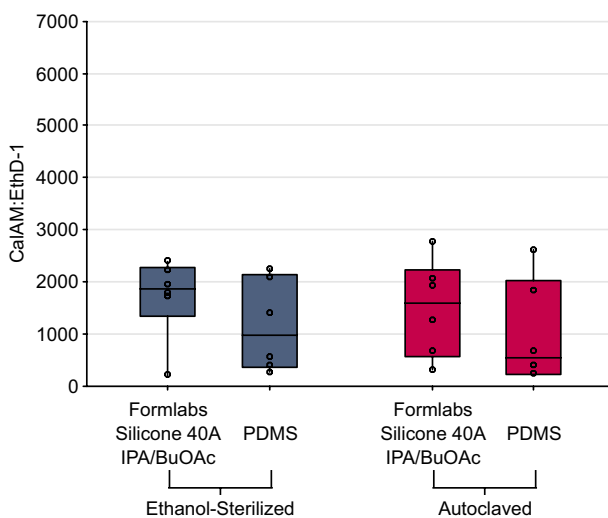


**Fig. 7** The CalAM:EthD-1 responses represented as boxplots of the ethanol/UV-sterilized (dark blue-gray) and autoclaved (dark pink) Formlabs Silicone 40A post-treated with IPA/BuOAc samples and its associated PDMS reference standard samples. Open circles (○) represent individual data points. None of the individual data points were outliers. The upper and lower boundaries of the box represent the first and third quartiles. Whiskers extend from the interquartile boxes to the minimum and maximum values, excluding outliers.

with calcein AM and ethidium homodimer-1 (refer to Section [Cytotoxicity \(Plate Reader and Imaging\)](#)) appeared to qualitatively impact C2C12 morphology. However, since all of the quantitative analysis was conducted using fluorescence intensity ratios, the change in morphology should not impact the cytotoxicity analysis since healthy morphology was observed in the cell-only (blank) controls before the dye was loaded (Figs. 3, 4). Overall, since the microscopy images of the controls qualitatively demonstrated the expected fluorescence, further quantitative analyses on the fluorescence measurements using the plate reader (Figs. 5, 6, 7) can be completed to compare the potential cytotoxic impacts of each resin sample.

**Materials Characterization.** *Mechanical Testing Raw Data Exclusion Criteria.* During the mechanical testing process, the MTS C42 was programmed to automatically stop the session once the material sample broke or when the physical limit (force or displacement) was reached. However, in some trials, the machine did not detect the break. In other trials, the sample was improperly loaded and slipped from the grips securing the sample to the machine. To ensure these conditions did not impact the calculation of material properties, such as Young's modulus, select trials and data points where these exclusion events occurred were removed prior to fitting the data to material models:

1. Trials in which samples slipped during the testing procedures were excluded, as indicated by the “Use Sample” column in the “Specific Geometries” sheet in the “masterRawData\_clean.xlsx” document (1: use test, 0: exclude test).
2. Time points after the failure of a sample (indicated by a large, sudden drop in the force) were removed, leaving all data from before the break. The data from before the failure that were used to calculate mechanical properties are located in the “Compression\_Rem” and “Tensile\_Rem” sheets.

**Effect of PBS Soak on Mechanical Properties.** For both Liqcreate Bio-Med Clear and Phrozen AquaGray 8K, the Young's moduli that were measured from our nonsterile tensile tests were consistently lower than those reported by the manufacturer (Table 6). Asiga did not report a modulus for their DentaGUIDE resin, so this same observation could not be made. We suspected that this decrease in nonsterilized Young's modulus was due to the 16-hour soak in 37°C PBS to which all samples were subjected prior to mechanical tests. To validate this, we conducted follow-up experiments on pre-curved cantilevered beams as outlined above (See Sec. Effect of PBS Pre-Soaking). Beams that were not soaked in PBS had Young's moduli much closer to values reported by the manufacturers (Table 6), whereas beams that were soaked were in much better agreement with values measured during the experiments reported here. Thus the metrics measured from these experiments should be interpreted in the context of PBS-soaked parts. The mechanical properties and the effects of different sterilization techniques on these resins when not soaked are beyond the scope of this current work. However, as the goal of this work is to investigate these properties for use in biohybrid robotics contexts, where these materials will be in consistent contact with similar saline solutions to protect the biological components, the mechanics under the soaked conditions as presented here, rather than the unsoaked data from the manufacturers, should be used in the biohybrid design process.

**Print Fidelity Manual Scorer Variance.** Due to the manual nature of the print feature quality assessment, there is inherent variation between individual scorers. The variation accounted for by the individual scorers was

Feature	<i>p</i> -value
Column Containing the Largest Feature	0.231
Column Containing the Smallest Feature	0.161
Row Containing the Largest Feature	0.181
Row Containing the Smallest Feature	0.160
Print Fidelity (Entire Sample)	0.160
Print Fidelity (Quadrant 1)	0.160
Print Fidelity (Quadrant 2)	0.167
Print Fidelity (Quadrant 3)	0.176
Print Fidelity (Quadrant 4)	0.162

**Table 7.** The *p*-values generated using a mixed effects model for the print fidelity data to determine whether the individual scorer significantly impacted the response of each manually scored feature. A  $p \leq \alpha = 0.05$  was used as the criterion to reject the null hypothesis where there is no relationship between the scorer identification and the measured response (feature).

assessed using a mixed effects model in Minitab 2024 (v 22.1), with the categorical factors of sterilization type, resin type, and interaction between sterilization and resin type and the random factor as the individual scorer identification. While the scoring responses were not continuous, Likert-type scale responses can be assessed using parametric tests<sup>32</sup>. A significance level  $\alpha$  of 0.05 was selected for these analyses, with a  $p \leq \alpha$  used as the criterion to reject the null hypothesis, where the null hypothesis is that there is no relationship between the factors and response. Using this mixed effects model, the individual scorer identification was found to not have a statistically significant effect on the variation in print fidelity (Table 7). Therefore, the manual scores can be used to assess the impacts on the final feature quality due to the combination of sterilization treatment and the low-cost 3D printing protocol for each resin evaluated in this dataset.

### Usage Notes

With three different major analyses (cytotoxicity, mechanical properties, print fidelity) conducted on commercially available resins that undergo standard sterilization procedures, this data can be used in part or in whole. The comprehensive dataset was generated as a resource for materials selection in the design of biohybrid actuators. Parts of the dataset can also be used in other contexts, given that the intended application conditions closely align with the experimental conditions used for generating this dataset. This dataset could be used to identify materials for developing custom cell culture apparatuses that interface with C2C12 cells, tools that are regularly submerged in saline solutions, or items that may have short-term exposure to sterilization-like conditions.

### Code availability

MATLAB code was used to establish the mechanical models for each resin. All of the code can also be found in the same Zenodo repository<sup>31</sup> as the data and CAD files at <https://doi.org/10.5281/zenodo.15801032>.

Received: 24 February 2025; Accepted: 31 July 2025;

Published online: 13 August 2025

### References

- Ricotti, L. *et al.* Biohybrid actuators for robotics: A review of devices actuated by living cells. *Science Robotics* 2(12), 0495, <https://doi.org/10.1126/scirobotics.aaq0495> (2017).
- Wang, C., Zhang, Z., Wang, J., Wang, Q., Shang, L. Biohybrid materials: Structure design and biomedical applications. *Materials Today Bio* 16, 100352 <https://doi.org/10.1016/j.mtbio.2022.100352> Accessed 2024-05-20 (2022).
- Liao, A. S. *et al.* Biocompatibility of Asiga Dental Resins Using a Low-Cost Printer for Biohybrid Actuator Applications. In: Szczecinski, N. S., Webster-Wood, V., Tresch, M., Nourse, W. R. P., Mura, A., Quinn, R. D. (eds.) *Biomimetic and Biohybrid Systems* vol. 14930, pp. 399–412. Springer, Cham. [https://doi.org/10.1007/978-3-031-72597-5\\_27](https://doi.org/10.1007/978-3-031-72597-5_27). Series Title: Lecture Notes in Computer Science. Accessed 2024-12-26 (2025).
- Guttridge, C., Shannon, A., O'Sullivan, A., O'Sullivan, K. J., O'Sullivan, L. W. Biocompatible 3D printing resins for medical applications: A review of marketed intended use, biocompatibility certification, and post-processing guidance. *Annals of 3D Printed Medicine* 5, 100044 <https://doi.org/10.1016/j.jstm.2021.100044> Accessed 2023-11-30 (2022).
- International Organization for Standardization ISO 10993-1:2018: Biological evaluation of medical devices Part 1: Evaluation and testing within a risk management process <https://www.iso.org/standard/68936.html> (2018).
- Dai, Z., Ronholm, J., Tian, Y., Sethi, B., Cao, X. Sterilization techniques for biodegradable scaffolds in tissue engineering applications. *Journal of Tissue Engineering* 7, 204173141664881 <https://doi.org/10.1177/2041731416648810> Accessed 2024-05-31 (2016).
- Formlabs Guide to Resin 3D Printers: SLA vs. DLP vs. MSLA vs. LCD Accessed 2024-06-09 <https://formlabs.com/blog/resin-3d-printer-comparison-sla-vs-dlp/> (2024).
- Lalwani, C. LCD vs. DLP vs. SLA: Which 3D Printer is Best For You Accessed 2024-06-09 <https://phrozen3d.com/blogs/guides/sla-vs-dlp-vs-lcd-which-resin-3d-printer-is-the-best-for-you> (2020).
- Asiga Max X - Asiga <https://www.asiga.com/max-x/> (2024).
- Systems, D. Asiga MAX X Accessed 2024-04-10 <https://www.3d-printer.com/products/asiga-max-x/163943000017772029> (2019).
- Formlabs Form 3B+ Accessed 2024-04-10 <https://formlabs.com/3d-printers/form-3b/> (2024).
- Phrozen Phrozen Resin User Guide: Aqua 8K Series Resin - Gray / Red-Clay / Vanilla / Snow Gray. [https://cdn.shopify.com/files/1/0436/6965/1618/files/User\\_Guide\\_Aqua\\_8K\\_V4\\_Resin\\_EN.pdf?r=1708149717](https://cdn.shopify.com/files/1/0436/6965/1618/files/User_Guide_Aqua_8K_V4_Resin_EN.pdf?r=1708149717).
- 3Dresyns Power difference of DLP, LCD & MLCD printers and its consequences <https://www.3dresyns.com/pages/power-difference-of-dlp-lcd-mlcd-printers-and-its-consequences> (2024).

15. Liao, A. S. *et al.* Cytotoxicity and characterization of 3d-printable resins using a low-cost printer for muscle-based biohybrid devices. bioRxiv <https://doi.org/10.1101/2024.10.31.621115> (2024).
16. Formlabs Formlabs Form 4 vs. Phrozen Sonic Mini 8K & Mighty 12K <https://formlabs.com/compare/form-4-vs-phrozen-sonic> (2025).
17. International Organization for Standardization ISO 10993-5:2009: Biological evaluation of medical devices Part 5: Tests for in vitro cytotoxicity <https://www.iso.org/standard/36406.html> (2009).
18. International Organization for Standardization ISO 10993-12:2021: Biological evaluation of medical devices Part 12: Sample preparation and reference materials <https://www.iso.org/standard/75769.html> (2021).
19. Miranda, I. *et al.* Properties and applications of PDMS for biomedical engineering: A review **13** (1), 2 <https://doi.org/10.3390/jfb13010002> Accessed 2025-06-26.
20. Regehr, K.J. *et al.* Biological implications of polydimethylsiloxane-based microfluidic cell culture **9**(15), 2132 <https://doi.org/10.1039/b903043c> Accessed 2025-06-26.
21. Carter, S.-S.D. *et al.* PDMS leaching and its implications for on-chip studies focusing on bone regeneration applications **2**, 100004 <https://doi.org/10.1016/j.ooc.2020.100004> Accessed 2025-06-26.
22. Bagdasarian, I. A., Tonmoy, T. I., Park, B. H. & Morgan, J. T. In vitro formation and extended culture of highly metabolically active and contractile tissues **18**(11), 0293609 <https://doi.org/10.1371/journal.pone.0293609> Accessed 2025-06-26.
23. Schätzlein, E. & Blaeser, A. Recent trends in bioartificial muscle engineering and their applications in cultured meat, biorobotic systems and biohybrid implants **5**(1), 737 <https://doi.org/10.1038/s42003-022-03593-5> Accessed 2025-06-26.
24. Monge, C. *et al.* Engineering muscle tissues on microstructured polyelectrolyte multilayer films **18**(15), 1664–1676 <https://doi.org/10.1089/ten.tea.2012.0079> Accessed 2025-06-26.
25. Molecular Probes LIVE/DEAD® Viability/Cytotoxicity Kit \*for mammalian cells\*. Molecular Probes <https://assets.thermofisher.com/TFS-Assets> (2005).
26. Gantentein-Ritter, B. *et al.* Accuracy of Three Techniques to Determine Cell Viability in 3D Tissues or Scaffolds. *Tissue Engineering Part C: Methods* **14**(4) 353–358 <https://doi.org/10.1089/ten.tec.2008.0313> Accessed 2024-06-10 (2008).
27. Yeoh, O. H., Fleming, P. D. A new attempt to reconcile the statistical and phenomenological theories of rubber elasticity. *Journal of Polymer Science Part B: Polymer Physics* **35**(12) 1919–1931 Accessed 2024-05-26 (1997).
28. Rohatgi, A. Webplotdigitizer: Version 4.6 <https://automeris.io/WebPlotDigitizer> (2022).
29. Voesenek, C. J., Li, G., Muijres, F. T. & Leeuwen, J. L. Experimental-numerical method for calculating bending moments in swimming fish shows that fish larvae control undulatory swimming with simple actuation. *PLoS Biology* **18**(7), 1–24, <https://doi.org/10.1371/journal.pbio.3000462> (2020).
30. Sun, X., Kerschen, G. & Cheng, L. Geometrical nonlinearities in a curved cantilever beam: a condensation model and inertia-induced nonlinear features. *Nonlinear Dynamics* **111**(7), 6533–6556, <https://doi.org/10.1007/s11071-022-08162-3> (2023).
31. Liao, A.S. *et al.* CMU-BORG/Commercial-Resins-for-Biohybrids-SciData: v1.1.0. Zenodo <https://doi.org/10.5281/zenodo.15801032> (2025).
32. Sullivan, G. M., Artino, A. R. Analyzing and Interpreting Data From Likert-Type Scales. *Journal of Graduate Medical Education* **5**(4) 541–542 <https://doi.org/10.4300/JGME-5-4-18> Accessed 2024-05-23 (2013).
33. Choi, J.J.E., Chen, S., Waddell, J.N. Investigation of dental elastomers as oral mucosa simulant materials. *Clinical and Experimental Dental Research* **7**(5) 754–762 <https://doi.org/10.1002/cre2.399> Accessed 2024-06-09 (2021).
34. Liqcreate Bio-Med Clear <https://www.liqcreate.com/product/bio-med-clear-biocompatible-resin/> (2024).
35. Formlabs Silicone 40A Resin Accessed 2024-05-30 <https://formlabs.com/store/materials/silicone-40a-resin/> (2024).
36. 3Dresyns 3Dresyn Bioflex A10 MB Monomer Based <https://www.3dresyns.com/products/3dresyn-bioflex-a10-mb-monomer-based> (2024).
37. Formlabs Silicone 40A Resin (Rev. 02). <https://media.formlabs.com/m/2e6bb2b3d645b427/original/-ENUS-Silicone-40A-TDS.pdf>.
38. Asiga Materials Dental - Asiga <https://www.asiga.com/materials-dental/> (2024).

## Acknowledgements

This material is based upon work supported by the National Science Foundation (NSF). ASL, SS, and MJB were supported by the Graduate Research Fellowship Program under Grant No. DGE1745016. This work was also supported by the NSF Faculty Early Career Development Program under Grant No. ECCS-2044785. Any opinions, findings, and conclusions or recommendations expressed in this material are those of the author(s) and do not necessarily reflect the views of the National Science Foundation. Research was sponsored by the Army Research Office and was accomplished under Cooperative Agreement Number W911NF-23-2-0138. The views and conclusions contained in this document are those of the authors and should not be interpreted as representing the official policies, either expressed or implied, of the Army Research Office or the U.S. Government. The U.S. Government is authorized to reproduce and distribute reprints for Government purposes notwithstanding any copyright notation herein. The authors were also supported in part by a PMFI (Pennsylvania Manufacturing Fellows Initiative) grant. KD was also supported by the Innovation Commercialization Fellowship from Carnegie Mellon University. ABI gratefully acknowledges financial support for this publication by the Fulbright Post Doctoral Program, which is sponsored by the U.S. Department of State and Turkish Fulbright Commission.

## Author contributions

Ashlee S. Liao: Conceptualization, Methodology, Software, Validation, Formal Analysis, Investigation, Resources, Data Curation, Writing - Original Draft, Writing - Review & Editing, Visualization, Supervision, Project Administration, Funding Acquisition. Kevin Dai (Equal Contributions to A.B.I.): Conceptualization, Methodology, Validation, Investigation, Resources, Writing - Review & Editing, Funding Acquisition. Alaeddin Burak Irez (Equal Contributions to K.D.): Conceptualization, Methodology, Validation, Investigation, Data Curation, Writing - Original Draft, Writing - Review & Editing, Funding Acquisition. Anika Sun (Equal Contributions to M.J.B.): Methodology, Software, Validation, Formal Analysis, Investigation, Data Curation, Writing - Original Draft, Writing - Review & Editing, Visualization. Michael J. Bennington (Equal Contributions to A.S.): Methodology, Software, Formal Analysis, Data Curation, Writing - Original Draft, Writing - Review & Editing, Visualization. Saul Schaffer: Methodology, Investigation, Writing - Review & Editing, Funding Acquisition. Bhavya Chopra: Methodology, Investigation, Writing - Review & Editing. Ji Min Seok: Methodology, Investigation, Writing - Review & Editing. Rebekah Adams: Investigation, Writing - Review & Editing. Yongjie Jessica Zhang: Writing - Review & Editing, Supervision, Funding Acquisition. Victoria A. Webster-Wood:

Conceptualization, Methodology, Validation, Formal Analysis, Resources, Data Curation, Writing - Review & Editing, Visualization, Supervision, Project Administration, Funding Acquisition.

### Competing interests

The authors declare no competing interests.

### Additional information

**Correspondence** and requests for materials should be addressed to V.A.W.-W.

**Reprints and permissions information** is available at [www.nature.com/reprints](http://www.nature.com/reprints).

**Publisher's note** Springer Nature remains neutral with regard to jurisdictional claims in published maps and institutional affiliations.



**Open Access** This article is licensed under a Creative Commons Attribution-NonCommercial-NoDerivatives 4.0 International License, which permits any non-commercial use, sharing, distribution and reproduction in any medium or format, as long as you give appropriate credit to the original author(s) and the source, provide a link to the Creative Commons licence, and indicate if you modified the licensed material. You do not have permission under this licence to share adapted material derived from this article or parts of it. The images or other third party material in this article are included in the article's Creative Commons licence, unless indicated otherwise in a credit line to the material. If material is not included in the article's Creative Commons licence and your intended use is not permitted by statutory regulation or exceeds the permitted use, you will need to obtain permission directly from the copyright holder. To view a copy of this licence, visit <http://creativecommons.org/licenses/by-nc-nd/4.0/>.

© The Author(s) 2025